UWB On-Body Radio Channel Modeling Using Ray Theory and Subband FDTD Method

Yan Zhao, *Student Member, IEEE*, Yang Hao, *Member, IEEE*, Akram Alomainy, *Student Member, IEEE*, and Clive Parini, *Member, IEEE*

***Abstract*—This paper presents the ultra-wideband on-body radio channel modeling using a subband finite-difference time-domain (FDTD) method and a model combining the uniform geometrical theory of diffraction (UTD) and ray tracing (RT). In the subband FDTD model, the frequency band (3–9 GHz) is uniformly divided into 12 subbands in order to take into account the material frequency dispersion. Each subband is simulated separately and then a combination technique is used to recover all simulations at the receiver. In the UTD/RT model, the RT technique is used to find the surface diffracted ray path, while the UTD is applied for calculating the received signal. Respective modeling results from two- and three-dimensional subband FDTD and UTD/RT models indicate that antenna patterns have significant impacts on the on-body radio channel. The effect of different antenna types on on-body radio channels is also investigated through the UTD/RT approach.**

***Index Terms*—Finite difference time domain (FDTD), on-body, ray tracing (RT), ultra-wideband (UWB), uniform geometrical theory of diffraction (UTD).**

I. Introduction

NEXT-GENERATION wireless and mobile systems are evolving toward personal and user-centric networks, where constant and reliable connectivity and services are essential. The idea of a number of nodes scattered around the human body and communicating wirelessly with each other sounds appealing and promising to many technologists and developers. This has led to the rapid increase in studies on wireless body area networks (WBANs). One promising application is patient monitoring, where the user is no longer restricted to a specified place, which results in faster recovery and less expensive treatment at any time. Other applications of wireless body-centric networks include wearable entertainment systems and high performance mobile PCs.

For low-power, reliable, and robust on-body communication systems, a deterministic and generic channel model is required to provide a clearer picture of the on-body radio propagation and its behavior with regards to different environments and system components. There have been a number of literatures characterizing and analyzing the on-body channel and also investigating the electromagnetic wave propagation around the body [1]–[6]. However, to the authors' knowledge, ultra-wideband (UWB) on-body radio channels have not been well studied due to the difficulty in characterizing frequency-dependent electrical properties of human tissues and other effects from antenna types and body movements, etc.

The conventional and empirical channel models available for many narrowband and wideband systems are insufficient to describe UWB channel behavior due to the UWB nature of the transmitted signals. The ray tracing (RT) technique and FDTD method have been widely studied and applied to indoor/outdoor propagation modeling for narrowband and UWB systems. Sarkar *et al.* presented a survey of various propagation models for mobile communications [7]. Wang *et al.* introduced a hybrid technique based on the combination of RT and FDTD methods for narrowband systems [8]. Recently, Attiya and Safaai-Jazi proposed a simulation model for UWB indoor radio channels using RT [9]. For UWB on-body radio channel modeling, Fort *et al.* simulated pulse propagation around the torso at the frequency range 2–6 GHz using Remcom XFDTD [10]. However, the variation of UWB on-body channel at different frequencies caused by material dispersion was not taken into account. In this paper, we present a novel deterministic on-body channel model using a subband finite-difference time-domain (FDTD) method. Numerical results obtained are compared with those from a hybrid uniform geometrical theory of diffraction (UTD)/RT model. The main advantage of the proposed subband FDTD over UTD/RT is its accuracy when modeling complicated on-body radio channels at an UWB frequency band. Compared with the dispersive FDTD, although the dispersive FDTD has been developed to model general dispersive materials, the determination of the coefficients for the rational functions to fit measurement data requires further effort such as applying the Padé approximations or the frequency-domain Prony method (FDPM) [11], [12]. The subband approach can be directly applied to different human tissues with any type of frequency dependence.

This paper is organized as follows. Section II introduces the measurement setup for UWB on-body radio channels, and results will be used for the evaluation of proposed channel models, Section III proposes the subband FDTD and UTD/RT model for UWB on-body channels. Section IV presents numerical results and their comparison with the measurement. Section V draws a conclusion.

II. Measurement Setup

The Fourier-transform relation between time- and frequency-domain signals allows the measurement of channel impulse responses (CIRs) using a frequency-domain sounding setup. The

Manuscript received August 10, 2005; revised January 13, 2006.

The authors are with the Department of Electronic Engineering, Queen Mary College, University of London, London E1 4NS, U.K. (e-mail: y.hao@elec.qmul.ac.uk).

Digital Object Identifier 10.1109/TMTT.2006.872072

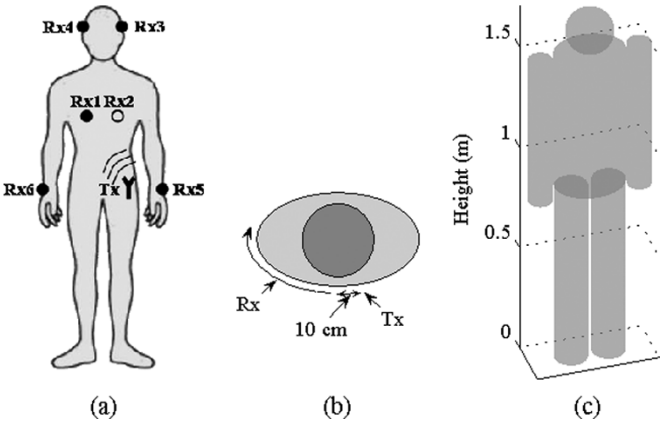

Fig. 1. 2-D and 3-D human body models. (a) Antenna positions for on-body radio channel modeling and measurement. (b) 2-D ellipse cylinder used for modeling both transmitter and receiver mounted on the trunk. (c) 3-D human body model used in both subband FDTD and UTD/RT models.

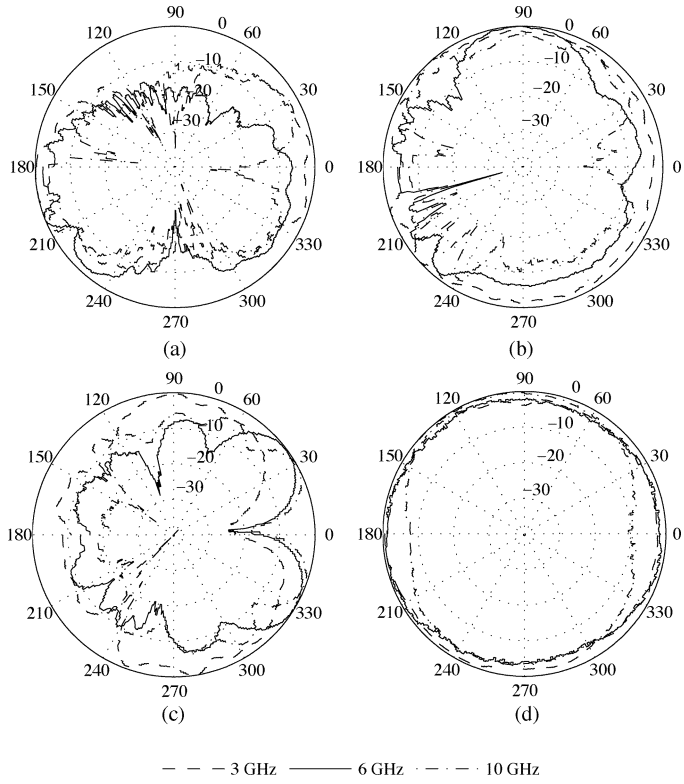

Fig. 2. Measured radiation patterns at 3, 6, and 10 GHz for HSCA. (a) E-field. (b) H-field and PICA. (c) E-field. (d) H-field. The solid line (6 GHz) is the curve used in UTD/RT model.

radio propagation channel measurement in the frequency domain has been proven [13], [14] to be accurate as several time-domain techniques if real-time signals are not required and long distances not included.

A vector network analyzer (VNA) is used to measure the $S21$ (complex frequency responses) of the on-body UWB channel covering the frequency band of 3–9 GHz with intervals of 3.75 MHz at a sweeping rate of 800 ms over 1601 assigned tones. Measurement settings and procedure are detailed in [4] and [15]. Various on-body antenna positions and different body postures are applied to obtain a deterministic UWB channel model. Fig. 1(a) shows the transmitting and receiving antenna positions as placed during measurement for the characterization of different on-body links. 710 frequency responses are collected for post measurement analysis and data processing. Two sets of measurements are performed in the anechoic chamber. The UWB antennas used for the on-body measurement campaign are the printed horn shaped self-complementary antenna (HSCA) and planar inverted cone antenna (PICA). The antennas are designed and fabricated following the description outlined in [4] and [15]. HSCA exhibits approximately constant impedance and absolute gain across the UWB band. The PICA antenna provides outstanding impedance and radiation pattern performance with gain of 0–3 dBi [4], [15]. Comparing the far-field radiation patterns for both the azimuth plane and elevation plane, in Fig. 2, the two antennas at different frequencies shows that better radiation bandwidth is obtained for the PICA case in comparison to the HSCA case. During the path loss measurement around the trunk [see Fig. 1(b)], the printed PICA is used and placed conformal to the body; for the whole body channel measurement [see Fig. 1(a)], PICA and HSCA are used and placed normal and conformal to the body surface, respectively. The effects of antenna types on the on-body UWB channels are analyzed and investigated in details in [4] and [15] with modeling aspects discussed intensively in this paper.

III. Modeling Techniques

The main aim of this study is to investigate on-body radio channels and develop appropriate modeling tools. In this paper, the on-body channel is modeled in a free-space environment and compared with measurements performed in an anechoic chamber. A wideband Gaussian monocycle is chosen as the pulse excitation [16]: in the subband FDTD model, different pulses are used according to the center frequency of each subband; for the UTD/RT, a single pulse of central frequency at 6 GHz is used.

A. Subband FDTD Model

In UWB radio channels, the inherent material dispersions represent the changes of permittivity and conductivity, etc. with frequency. Such dispersions cannot be directly modeled using existing dispersive FDTD based on Debye/Lorentz relations. To apply the subband FDTD method, one can follow the below steps [17], [18].

Step 1) First divide the whole frequency band into several subbands, each of which is narrow enough to assume same frequency characteristics.

Step 2) Use the conventional FDTD method to obtain the time-domain delay profiles for each subband.

Step 3) Then Fourier transform subband delay profiles into the frequency domain; extract the "accurate" part and combine them to have a new frequency response.

Step 4) Finally, transform the frequency responses back into the time domain to have a delay profile that is valid over the entire UWB.

The choice of the number of subbands depends on the accuracy requirement to approximate dispersive material properties.

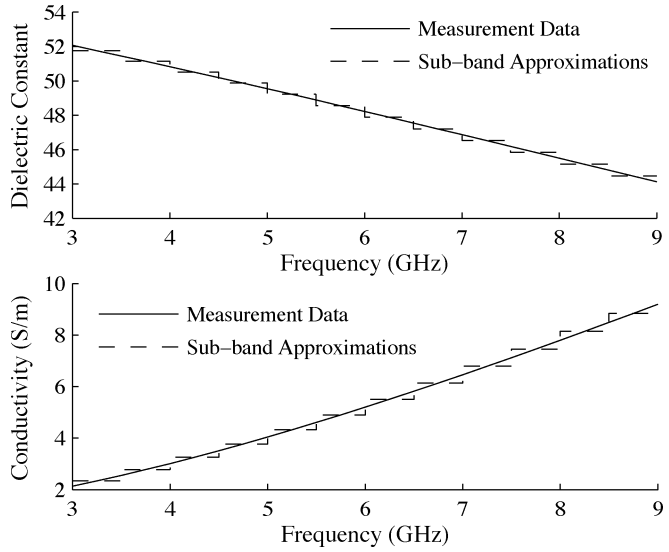

Fig. 3. Measured permittivity and conductivity of human muscle in the UWB band and subband approximations for the subband FDTD model.

Generally, the greater the number of subbands, the more accurate the subband FDTD model is. However, since each subband needs to be simulated separately, as the number of subbands increases, further simulation efforts are required. For our on-body propagation analysis, sufficient accuracy can be ensured by dividing the whole frequency band (3–9 GHz) into 12 subbands with 500-MHz bandwidth for each subband. For instance, the relative dielectric constant of human muscle ranges from 52.058 at 3 GHz to 44.126 at 9 GHz.[1] Twelve subbands are used to match the frequency-dispersion curve by assuming the dielectric constant within each subband to be constant (obtained at the center frequency of each subband). The overall error from such a curve fitting is less than 1%. Fig. 3 shows the frequency-dependent dielectric constant and conductivity of human muscle from measurement and their staircasing approximations used in the proposed subband FDTD model.

For Step 3), the combination of received signals in the frequency domain can be obtained using (1) as follows:

$$F_r(\omega) = \sum_{i=1}^{N} F_{r,i}(\omega) \cdot A_i(\omega) \tag{1}$$

where $F_{r,i}(\omega)$ is the received frequency-domain signal at the ith subband, $A_i(\omega)$ is a rectangle window function associated with the bandwidth of the ith subband, and N is the total number of subbands. Finally, the combined frequency-domain signal is inverse Fourier transformed into the time domain to obtain a time-delay profile.

Although the FDTD method has been successfully applied to the antenna design [19] for various applications, the inclusion of antenna patterns, etc. in radio propagation analysis using a global FDTD method is not feasible due to the constrains of limited computer resources. In this paper, the antenna is approximated as a point source of narrow Gaussian pulse and it is viable in particular for PICA, which radiates almost omni-directionally across the frequency band.

[1]An Internet resource for the calculation of the dielectric properties of body tissues, Inst. Appl. Phys., Italian Nat. Res. Council, Florence, Italy. [Online]. Available: http://niremf.ifac.cnr.it/tissprop/

B. UTD/RT Model

Basic RT techniques include two approaches, i.e., the image method [20] and the method of shooting and bouncing rays (SBR) [21]. In the UTD/RT model proposed in this paper, the SBR method is used. When the on-body channel is modeled using the hybrid UTD/RT approach, the RT is used to find the surface ray path while the UTD is applied for calculating surface diffracted signal strength. In [22], it has been shown that the human body can be modeled as a metallic cylinder regardless of its associated dielectric parameters. In our UTD/RT model, conducting sphere and cylinders are used to represent different parts of the human body and, thus, the UTD surface diffraction coefficients [23] can be used. The UTD solutions for a radiation problem in the shadow zone are given by (2) and (3) as follows:

$$\mathbf{E}^d(P_d) = C_0 Z \mathbf{J}(Q') \cdot \hat{\mathbf{n}}(Q')\hat{\mathbf{n}}(Q) H(\xi_c) \times \left[\frac{a_0(Q)}{a_0(Q')}\right]^{\frac{1}{6}} e^{-jkt} \frac{e^{-jks^d}}{\sqrt{s^d}} \tag{2}$$

for the electric current source and

$$\mathbf{E}^d(P_d) = C_0 \mathbf{M}(Q') \cdot \left[\hat{\mathbf{b}}\hat{\mathbf{n}}(Q) H(\xi_c) + \hat{\mathbf{t}}(Q')\hat{\mathbf{b}} S(\xi_c)\right] \times \left[\frac{a_0(Q)}{a_0(Q')}\right]^{\frac{1}{6}} e^{-jkt} \frac{e^{-jks^d}}{\sqrt{s^d}} \tag{3}$$

for the magnetic current source where $H^l(\xi)$ and $S^l(\xi)$ are defined in terms of the hard and soft Fock radiation functions. The UTD solutions for surface coupling problem are given by (4) and (5) as follows:

$$\mathbf{E}(Q) = C_0 Z \mathbf{J}(Q') \cdot [\hat{\mathbf{n}}(Q')\hat{\mathbf{n}}(Q)]\, F_s(\xi_c) e^{-jkt} \tag{4}$$

for the electric current source and

$$\mathbf{H}(Q) = C_0 Y \mathbf{M} \cdot \left[\hat{\mathbf{b}}(Q')\hat{\mathbf{b}}(Q) F_s(\xi_c) + \hat{\mathbf{t}}(Q')\hat{\mathbf{t}}(Q) G_s(\xi_c)\right] e^{-jkt} \tag{5}$$

for the magnetic current source where F_s applies to the TE coupling configuration and G_s is applicable to the TM situation. Other parameters and geometrical arrangements for calculating surface diffracted field in (2)–(5) are defined in [23]. Note that before tracing each ray, the associated field is first separated into a TE and a TM part, and then the surface diffracted field can be calculated in terms of each part and combined at the receiver.

For a simple 2-D case, as shown in Fig. 1(b) with given geometrical parameters and field polarization information, the UTD diffraction coefficient for a convex surface coupling problem can be directly used to calculate the diffracted field without the need for tracing rays at different directions. For the three-dimensional (3-D) scenario, as shown in Fig. 1(c), since the human

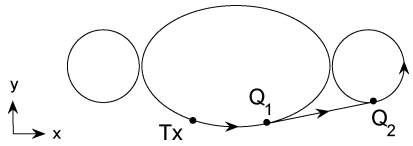

Fig. 4. 2-D view of surface diffracted ray path with the locations of the transmitter (Tx), the shedding point Q_1, and the attachment point Q_2.

body is modeled in free space, only the rays in the tangential plane at the transmitter need to be traced. Provided that the tracing plane does not intersect with other body parts besides the trunk, all the traced rays start with creeping waves. The procedure for finding the surface diffracted ray path can be summarized as follows.

Step 1) First establish a simplified 3-D human body model [see Fig. 1(c)] with all the required geometrical dimensions. Assign the locations of the transmitter and receiver.

Step 2) Generate the first ray at the initial tracing angle (0° to the horizontal plane) from the transmitter.

Step 3) Along the current ray direction, search for possible surface ray path (up to one surface diffraction) to the receiver according to the generalized Fermat principle [23]; search for possible reflected ray path (up to one reflection) to the receiver from other body parts.

Step 4) If any of the ray paths is present, use a UTD surface diffraction/reflection coefficient to calculate the diffracted/reflected signal strength.

Step 5) Search for another surface ray path on different body parts along the ray direction, as shown in Fig. 4, and repeat Step 3) until the associated field strength falls below a pre-specified threshold.

Step 6) Generate a new ray at a different angle (e.g., 0.5° increase) and start over from Step 3).

Note that from Step 3), multiple reflected rays are not taken into account in our UTD/RT model due to the complexity in finding a multiple reflected ray path for the on-body scenario. In Step 5), in order to find the surface ray path, the shedding point Q_1 and attachment point Q_2 are first calculated geometrically in a two-dimensional (2-D) $(x-y)$ plane (projection of 3-D), as illustrated in Fig. 4. The position of these points in the z-direction can then be calculated from the direction of the ray. At the receiver, each of the received rays contains the effect of multiple surface diffractions/single reflection from different body parts. The polarization information for calculating the diffracted field is obtained from the orientation of antennas placed in measurement.

The received frequency-domain signal can be calculated using (6) [23] as follows:

$$E(\omega)=\sum_{i=1}^{N} E_0(\omega)G_{ti}(\omega)G_{ri}(\omega)A_i\prod_j D_j(\omega)\prod_l R_l(\omega)e^{-j\frac{\omega}{c}d_i} \tag{6}$$

where $E_0(\omega)$ is the transmitted frequency-domain signal, $G_{ti}(\omega)$ and $G_{ri}(\omega)$ are the transmitting and receiving antenna field radiation patterns in the direction of the ith ray, A_i is a distance factor, $D(\omega)$ and $R(\omega)$ are the diffraction and reflection coefficients, j and l depend on the number of diffractions and reflections before reaching the receiver, respectively, $e^{-j(\omega/c)d_i}$ is the propagation phase factor due to the path length d_i, c is the speed of wave propagation, and N is the total number of received rays. Note that in our simulations, the frequency dependency of $G_{ti}(\omega)$ and $G_{ri}(\omega)$ in (6) is not taken into account and the patterns at 6 GHz for both antennas are used. Therefore, the frequency-domain behavior caused by the radiation process of UWB antennas [24] is not included in our analysis.

IV. Numerical Results and Analysis

The subband FDTD method is validated by comparing the reflection coefficient calculated from one-dimensional (1-D) subband FDTD simulation and analytical equations. The analytical equation is given by [25]

$$R(\omega)=\frac{1-e^{-j2\delta}}{1-R'^2(\omega)e^{-j2\delta}}R'(\omega) \tag{7}$$

where $\delta=(2\pi d/\lambda)\sqrt{n^2(\omega)-\sin^2(\theta)}$, λ is the wavelength in free space, d is the thickness of the dielectric plate, $n(\omega)$ is its complex and dispersive refractive index, and θ is the angle of incidence. In (7), $R'(\omega)$ is given by

$$R'_s(\omega)=\frac{\cos(\theta)-\sqrt{n^2(\omega)-\sin^2(\theta)}}{\cos(\theta)+\sqrt{n^2(\omega)-\sin^2(\theta)}} \tag{8}$$

or

$$R'_p(\omega)=\frac{n^2(\omega)\cos(\theta)-\sqrt{n^2(\omega)-\sin^2(\theta)}}{n^2(\omega)\cos(\theta)+\sqrt{n^2(\omega)-\sin^2(\theta)}} \tag{9}$$

where $R'_s(\omega)$ and $R'_p(\omega)$ are the Fresnel's reflection coefficients for the interface between air and a dielectric media whose frequency-dependent complex refractive index is $n(\omega)$ when the electric field is perpendicular and parallel to the incident plane, respectively.

For the 1-D subband FDTD simulation, 300 cells are used to model the free space and 100 cells for the dielectric slab (modeled as bricks with thickness 0.20 m), as shown in Fig 5(a). The cell size is 2.0×10^{-3} m and the time step is 3.3×10^{-12} s. The reflected signal is obtained by subtracting the direct signal from the total received signal and the wideband reflection coefficient is calculated by dividing the reflected and incident field strength in the frequency domain. As presented in Fig. 5(b), the comparison shows good agreement and validates the subband FDTD method.

A detailed comparison between different modeling techniques for indoor UWB radio propagation has been presented in [26]. When these techniques are applied to the UWB on-body communications, a simplified human body model is used with

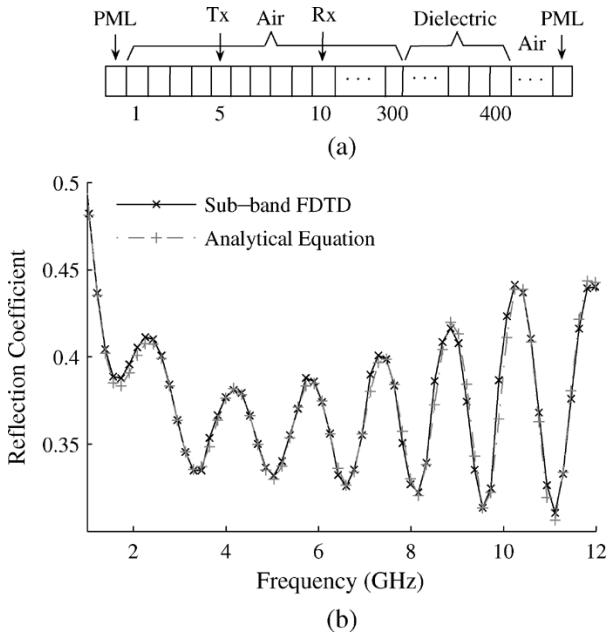

Fig. 5. (a) 1-D subband FDTD simulation domain. (b) Comparison of reflection coefficient for normal incidence at an air–brick interface calculated from the subband FDTD method and analytical equation.

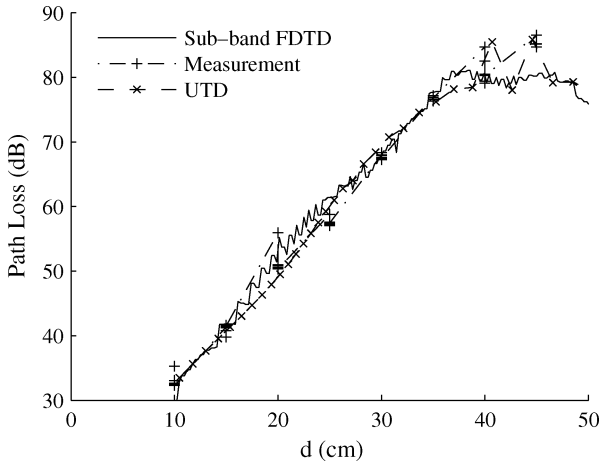

Fig. 6. Comparison of path losses along the trunk [see Fig. 1(b)] from the subband FDTD model, UTD model, and measurement.

only muscles are considered. The frequency-dependent dielectric constant and conductivity of human muscle can be found from measurement and is shown in Fig. 3.

A. 2-D On-Body Propagation Channels

Applying both subband FDTD and UTD/RT methods to a simple (2-D) scenario is first considered. Both the transmitter and receiver are mounted on the trunk. As the receiver moves along the trunk in the same horizontal plane, the scenario can be treated as a 2-D case. As shown in Fig. 1(b), the human body (trunk) is modeled as a 2-D ellipse cylinder with a semimajor axis of 0.15 m and semiminor axis of 0.12 m according to the dimensions of a human candidate volunteered in the measurement. Both the transmitter and receiver are placed on the "trunk" and the transmitter is 10 cm offset from the center. During the measurement, the receiver is always kept on the "trunk" while moving along the route, as shown in Fig. 1(b). The TM polarized field is considered for both subband FDTD and UTD/RT models due to the orientation and the radiated field of the antenna used in the measurement. The antenna pattern contribution is excluded in this analysis because, for any receiver location, the received signal only contains the contributions from two creeping waves traveling from the transmitter at opposite directions tangential to the ellipse's surface. While mutual coupling between transmitting and receiving antennas is considered [23], with given transmitter/receiver locations and geometrical dimensions (ellipse cylinder), the UTD diffraction coefficient for TM-polarized field can be directly used to calculate diffracted signal strength. The approximate elliptic "trunk" is also modeled using the subband FDTD with the cell size of 3.0×10^{-3} m. The number of cells in the computational region is 140×160, which is truncated by a ten-cell Berenger's perfect matched layer (PML) [27].

On-body path loss is calculated at different receiver locations using (10) as follows:

$$\mathrm{PL}(d) = -10 \log_{10} \left(\frac{E_r}{E_t} \right) \tag{10}$$

where E_t and E_t are the total transmitted and total received signal energy, respectively.

Fig. 6 shows the path-loss results along the trunk [see Fig. 1(b)] from the subband FDTD model, UTD/RT model, and measurement. Good agreement is achieved when the creeping distance of the transmitter and receiver is small. However, when the distance approaches the maximum, ripples are observed from UTD/RT and measurement, which are caused by the adding up or cancelling of two creeping rays traveling along both sides of the elliptical "trunk." The subband FDTD model fails to accurately predict such phenomenon due to the staircase approximation of the curved surfaces, and such a problem can be alleviated by using a conformal FDTD method [28]. Fig. 6 indicates that, for modeling simple on-body communication scenarios, such as both the transmitter and receiver are on the trunk, UTD is very efficient and provides accurate results.

B. 3-D On-Body Propagation Channels

Both the subband FDTD and UTD/RT are applied to model the UWB on-body radio channel in three dimensions. As shown in Fig. 1(a), different antenna positions are chosen due to locations of commonly used on-body communication devices such as head-mounted display, headset, and wristwatch, etc. The human body is modeled by several different geometries, i.e., one sphere for the head ($r = 0.10$ m), one ellipse cylinder for the trunk ($a = 0.15$ m, $b = 0.12$ m, $h = 0.65$ m), and four cylinders for arms ($r = 0.05$ m, $h = 0.70$ m) and legs ($r = 0.07$ m, $h = 0.85$ m) according to the measurement candidate's dimensions.

In the subband FDTD, the whole body model only consists of muscle with the dielectric constant and conductivity obtained from the measurement (Fig. 3). The modeling environment is free space, which is meshed by $140 \times 160 \times 630$ cells with each

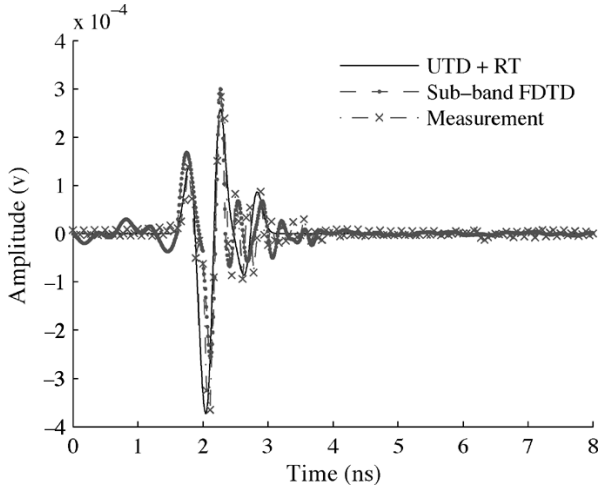

Fig. 7. Comparison of CIRs at Rx3 [see Fig. 1(a)] using PICA from the UTD/RT model, subband FDTD model, and measurement.

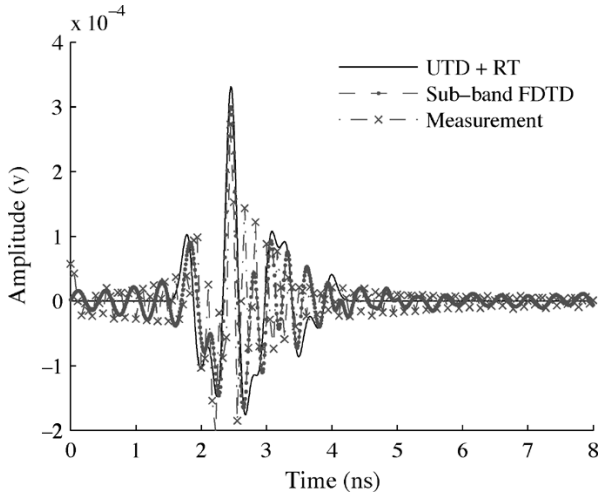

Fig. 8. Comparison of CIRs at Rx4 [see Fig. 1(a)] using PICA from the UTD/RT model, subband FDTD model, and measurement.

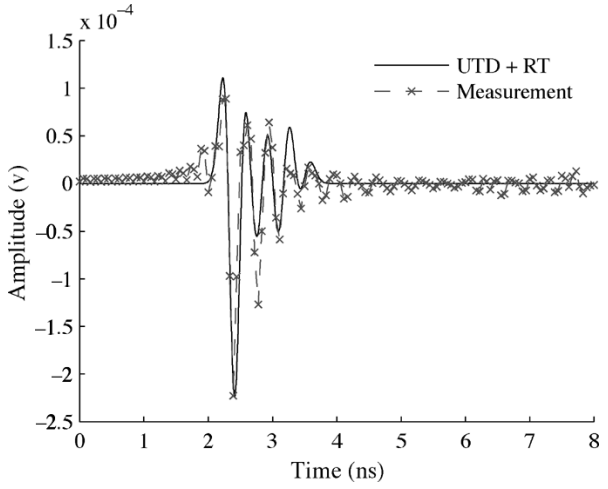

Fig. 9. Comparison of CIRs at Rx3 [see Fig. 1(a)] using HSCA from the UTD/RT model and measurement.

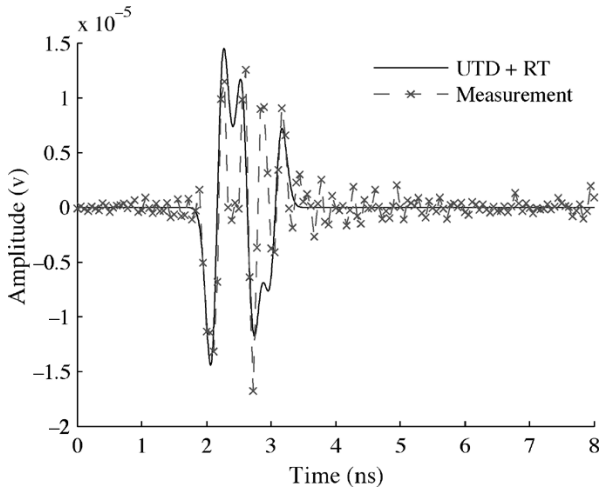

Fig. 10. Comparison of CIRs at Rx4 [see Fig. 1(a)] using HSCA from the UTD/RT model and measurement.

cell size 3.0×10^{-3} m. The time step is chosen as 5.0×10^{-12} s according to the stability criterion. The PICA is modeled as a point source due to its omni-directional radiation properties. The CIRs at two different receiver locations [Rx3 and Rx4 in Fig. 1(a)] are shown in Figs. 7 and 8.

In UTD/RT, the ray tube angle is set to be 0.5° for high accuracy [8]. The tracing of rays and the calculation of diffracted field are performed following the procedure introduced in Section III. Rays are terminated after their field strength drops 50 dB below the reference level. The threshold for on-body channel modeling is lower than that for indoor channel modeling (30 dB) due to the nonreflecting environment (free space) and relatively low amplitude of the received signal in our analysis. The CIRs at two different receiver locations [Rx3 and Rx4 in Fig. 1(a)] using two types of antennas (HSCA and PICA, Section II) from the UTD/RT model are shown in Figs. 7–10.

At the same receiver location [Rx3 or Rx4 in Fig. 1(a)], the CIR using PICA contains more multipath components compared with HSCA because of the difference between their radiation properties (Fig. 2). Using the same antenna at different receiver locations, for PICA (Figs. 7 and 8), the subband FDTD provides more accurate results (in terms of the number of multipath components) than UTD/RT compared with measurement since FDTD can fully account for the effects of reflection, diffraction, and radiation, while some rays are missing in the UTD/RT model compared with measurement; for HSCA, greater difference has been observed between UTD/RT and measurement at Rx4 (Fig. 10) compared with Rx3 (Fig. 9), which is due to the more complicated scenario caused by more severe body shadowing at Rx4, and higher order reflections/diffractions occur. For the subband FDTD model, the major difference between modeling results and measurements is caused by the approximation of the antenna by a point source, and the change of antenna radiation patterns at different frequencies. While for the UTD/RT model, the difference is due to the approximation of human tissue as a conducting material, and the change of antenna radiation patters at different frequencies.

In the local area of each receiver [Rx1–Rx6 for PICA and Rx1–Rx4 for HSCA, Fig. 1(a)], two more receiver locations

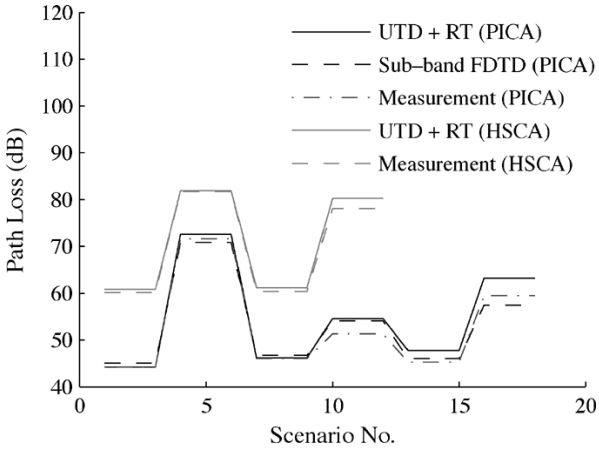

Fig. 11. Comparison of the average path loss around each receiver location for different on-body scenarios using PICA [Rx1–Rx6, Fig. 1(a)] and HSCA (Rx1–Rx4), respectively.

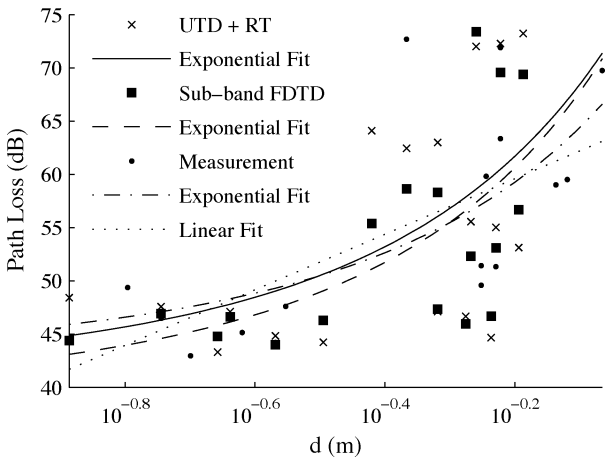

Fig. 12. Comparison of path loss for UWB on-body channels using PICA from UTD/RT model, subband FDTD model, and measurement. The exponential fitted curve for each model and the linear fitted line for measurement data are also shown.

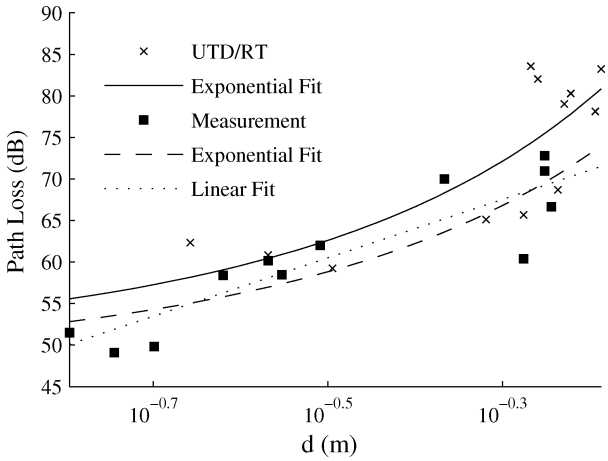

Fig. 13. Comparison of path loss for UWB on-body channels using HSCA from UTD/RT model and measurement. The exponential fitted curves and the linear fitted line for measurement data are also shown.

are considered, thus path-loss values at a total of 18 different locations are obtained. The average path loss is then calculated around each receiver location and compared with measurement results. Fig. 11 shows the comparison of average path loss for different on-body scenarios using PICA and HSCA, respectively. It can be seen that, for the distinctive on-body radio channel, the path-loss results from both subband FDTD and UTD/RT models are close to measurement.

A different least square (LS) fitting method can be used to fit the measurement and simulation data. In addition to the conventional linear power law fitting method, since the on-body channel mainly consists of creeping waves around the body, the exponential loss (decibels per meter) fitting might also be appropriate. The exponential fitting can be performed using (11) [29] as follows:

$$\mathrm{PL}(d) = Ae^{-\alpha d} \tag{11}$$

where A is the excitation coefficient and α is the attenuation coefficient. The linear power law fitting can be used to obtain the path-loss exponent γ through (12) as follows:

$$\mathrm{PL}(d) = \mathrm{PL}(d_0) + 10\gamma \log_{10}\left(\frac{d}{d_0}\right) + X_\sigma \tag{12}$$

where $\mathrm{PL}(d_0)$ is the reference path loss at distance d_0, γ is the path loss exponent, and X_σ is a zero-mean Gaussian random variable.

Figs. 12 and 13 show the comparison of path loss for different on-body channels using PICA and HSCA, respectively. The exponential fitted curves for different models and measurement are also shown. For comparison, the linear power law fitting is also performed for the measurement data. It can be seen that the exponential fitting is more appropriate for the data obtained due to the fact that the creeping wave is the dominant mechanism for the receiver locations considered in our models.

The values of excitation and attenuation coefficients for UTD/RT, subband FDTD models, and measurement for PICA and HSCA are listed in Tables I and II, respectively. For PICA, it can be seen that the UTD/RT model provides a closer match to measurement compared with the subband FDTD. In the UTD/RT model, the measured antenna pattern is used and the human body is approximated by conducting sphere and cylinders. In the subband FDTD model, although the material

TABLE I
VALUES OF EXCITATION AND ATTENUATION COEFFICIENTS FROM THE UTD/RT, SUBBAND FDTD MODELS, AND MEASUREMENT USING PICA

	UTD+RT	Sub-band FDTD	Measurement
Excitation coefficient	41.30	39.45	42.97
Attenuation coefficient	-0.64	-0.68	-0.51

TABLE II
VALUES OF EXCITATION AND ATTENUATION COEFFICIENTS FROM THE UTD/RT MODEL AND MEASUREMENT USING HSCA

	UTD+RT	Measurement
Excitation coefficient	49.14	47.31
Attenuation coefficient	-0.77	-0.69

frequency dispersion is considered, the antenna is approximated as a point source. The results indicate that the antenna pattern has a more important effect than the material frequency dispersion on the on-body channel. For HSCA, the difference is mainly caused by the change of the HSCA's radiation pattern at different frequencies and the approximation of the human body as conducting structures in the UTD/RT model.

V. Conclusion

On-body radio channel modeling has been performed using a subband FDTD and a combined UTD/RT model. In the subband FDTD model, the entire frequency band (3–9 GHz) has been first divided into 12 subbands with 500-MHz bandwidth for each subband in order to take into account the material frequency dispersion at different frequencies. Within each subband, the conventional FDTD has been applied to calculate the CIRs. A combination technique has been used at the receiver to recover all the subband simulations. The advantage of this method is its ability of modeling materials with any type of frequency dependence. In the UTD/RT model, the human body has been approximated by conducting sphere and cylinders, and the RT technique has been used together with the generalized Fermat principle to find a surface diffracted ray path, while the UTD surface diffraction coefficients are used for calculating the received signal strength. The proposed models have been applied to both 2-D and 3-D on-body scenarios and compared with measurement results. For cases such as when both a transmitter and receiver are mounted on the trunk, UTD/RT provides relatively simple and reliable solutions even if the human body is modeled as a conducting elliptic cylinder; while for a more complicated scenario, such as for the whole body channel modeling, the subband FDTD is capable of providing more general solutions due to its ability of fully accounting for the effects of reflection and diffraction. The modeling results indicate that the antenna pattern has significant impacts on on-body radio channels. Through the UTD/RT approach, the effect of different antenna types on on-body radio channels has also been investigated. The modeling results show good agreement with measurement.

Acknowledgment

The authors would like to thank the reviewers for their valuable comments and suggestions. The authors also thank J. Dupuy, Queen Mary College, University of London, London, U.K., for assistance with measurements.

References

[1] P. Hall, M. Ricci, and T. Hee, "Measurements of on-body propagation characteristics," in *Int. Microw. Millimeter-Wave Technol. Conf.*, 2002, pp. 770–772.

[2] T. Zasowski, F. Althaus, M. Stager, A. Witttneben, and G. Troster, "UWB for noninvasive wireless body area networks: Channel measurements and results," in *IEEE Ultra Wideband Syst. Technol. Conf.*, 2003, pp. 285–289.

[3] I. Kovacs, G. Pedersen, P. Eggers, and K. Olesen, "Ultra wideband radio propagation in body area network scenarios," in *Proc. ISSSTA*, 2004, pp. 102–106.

[4] A. Alomainy, Y. Hao, C. G. Parini, and P. S. Hall, "Comparison between two different antennas for UWB on-body propagation measurements," *IEEE Antennas Wireless Propag. Lett.*, vol. 4, no. 1, pp. 31–34, Dec. 2005.

[5] A. Alomainy, A. Owadally, Y. Hao, C. G. Parini, Y. Nechayev, C. C. Constantinou, and P. Hall, "Body-centric WLAN for future wearable computers," in *1st Int. Wearable Implantable Body Sens. Networks Workshop*, London, U.K., Apr. 6–7, 2004, pp. 42–44.

[6] Y. I. Nechayev, P. S. Hall, C. C. Constantinou, Y. Hao, A. Alomainy, R. Dubrovka, and C. G. Parini, "On-body path gain variations with changing body posture and antenna position," in *IEEE AP-S Int. Symp./USNC/URSI Nat. Radio Sci. Meeting*, Washington, DC, 2005, pp. 731–734.

[7] T. K. Sarkar, Z. Ji, K. Kim, A. Medour, and M. Salazar-Palma, "A survey of various propagation models for mobile communication," *IEEE Antennas Propag. Mag.*, vol. 45, no. 3, pp. 51–82, Jun. 2003.

[8] Y. Wang, S. Safavi-Naeini, and S. K. Chaudhuri, "A hybrid technique based on combining ray tracing and FDTD methods for site-specific modeling of indoor radio wave propagation," *IEEE Trans. Antennas Propag.*, vol. 48, no. 5, pp. 743–754, May 2000.

[9] A. M. Attiya and A. Safaai-Jazi, "Simulation of ultra-wideband indoor propagation," *Microw. Opt. Technol. Lett.*, vol. 42, no. 2, pp. 103–108, Jul. 20, 2004.

[10] A. Fort, C. Desset, J. Ryckaert, P. Doncker, L. Biesen, and S. Donnay, "Ultra wideband body area channel model," in *IEEE Int. Commun. Conf.*, May 2005, vol. 4, pp. 16–20.

[11] W. H. Weedon and C. M. Rappaport, "A general method for FDTD modeling of wave propagation in arbitrary frequency dispersive media," *IEEE Trans. Antennas Propag.*, vol. 45, no. 3, pp. 401–410, Mar. 1997.

[12] G. X. Fan and Q. H. Liu, "An FDTD algorithm with perfectly matched layers for general dispersive media," *IEEE Trans. Antennas Propag.*, vol. 48, no. 5, pp. 637–646, May 2000.

[13] S. J. Howard and K. Pahlavan, "Measurement and analysis of the indoor radio channel in the frequency domain," *IEEE Trans. Instrum. Meas.*, vol. 39, no. 5, pp. 751–755, Oct. 1990.

[14] H. Hashemi, "The indoor propagation channel," *Proc. IEEE*, vol. 81, no. 7, pp. 943–968, Jul. 1993.

[15] A. Alomainy, Y. Hao, X. Hu, C. G. Parini, and P. S. Hall, "UWB on-body radio propagation and system modeling for wireless body-centric networks," *Proc. Inst. Elect. Eng.–Commun.*, Jul. 2006, to be published.

[16] "Time modulated ultra-wideband for wireless applications," Time Domain Corporation, Huntsville, AL, PulsON Technol., May 2000.

[17] M. Terre, A. Hong, G. Guibe, and F. Legrand, "Major characteristics of UWB indoor transmission for simulation," in *Veh. Technol. Conf.*, Apr. 2003, pp. 19–23.

[18] H. Sugahara, Y. Watanabe, T. Ono, K. Okanoue, and S. Yarnazaki, "Development and experimental evaluations of 'RS-2000'—A propagation simulator for UWB systems," in *Joint Ultra Wideband Syst./ Ultra Wideband Syst. Technol. Conf.*, 2004, pp. 76–80.

[19] P. A. Tirkas and C. A. Balanis, "Finite-difference time-domain method for antenna radiation," *IEEE Trans. Antennas Propag.*, vol. 40, no. 3, pp. 334–340, Mar. 1992.

[20] M. C. Lawton and J. P. McGeehan, "The application of a deterministic ray launching algorithm for the prediction of radio channel characteristics in small-cell environments," *IEEE Trans. Veh. Technol.*, vol. 43, no. 4, pp. 955–969, Nov. 1994.

[21] H. Ling, R. C. Chou, and S. W. Lee, "Shooting and bouncing rays: Calculating the ROS of an arbitrary shaped cavity," *IEEE Trans. Antennas Propag.*, vol. 37, no. 2, pp. 194–205, Feb. 1989.

[22] M. Ghaddar, L. Talbi, and T. A. Denidni, "Human body modeling for prediction of effect of people on indoor propagation channel," *Electron. Lett.*, vol. 40, no. 25, pp. 1592–1594, Dec. 2004.

[23] D. A. McNamara, C. W. I. Pistorius, and J. A. G. Malherbe, *Introduction to the Uniform Geometrical Theory of Diffraction*. Norwood, MA: Artech House, 1990.

[24] K. Siwiak and D. McKeown, *Ultra-Wideband Radio Technology*. New York: Wiley, 2004.

[25] K. Sato, H. Kozima, H. Masuzawa, T. Manabe, T. Ihara, Y. Kasashima, and K. Yamaki, "Measurements of reflection characteristics and refractive indexes of interior construction materials in millimeter-wave bands," in *45th IEEE Veh. Technol. Conf.*, 1995, vol. 1, pp. 449–453.

[26] Y. Zhao, Y. Hao, and C. G. Parini, "Two novel FDTD based UWB indoor propagation models," in *IEEE Int. Ultra-Wideband Conf.*, Zurich, Switzerland, Sep. 5–8, 2005, pp. 124–129.

[27] J. R. Berenger, "A perfectly matched layer for the absorption of electromagnetic waves," *J. Comput. Phys.*, vol. 114, pp. 185–200, Oct. 1994.

[28] Y. Hao and C. J. Railton, "Analyzing electromagnetic structures with curved boundaries on Cartesian FDTD meshes," *IEEE Trans. Microw. Theory Tech.*, vol. 46, no. 1, pp. 82–88, Jan. 1998.

[29] L. Piazzi and H. L. Bertoni, "A path loss formulation for wireless applications considering terrain effects for urban environments," in *48th IEEE Veh. Technol. Conf.*, May 18–21, 1998, pp. 159–163.

Yan Zhao (S'03) received the B.Sc. degree in information engineering from the Beijing University of Posts and Telecommunications (BUPT), Beijing, China in 2002, and the M.Sc. degree in electronic, electrical, and computer engineering from The University of Birmingham, U.K., in 2003, and is currently working toward the Ph.D. degree at Queen Mary College, University of London, London, U.K.

In 2003, he joined the Department of Electronic Engineering, Queen Mary College, University of London. His main research interests include FDTD modeling of dispersive materials, UWB radio systems, and human interactions with indoor radio channels.

Yang Hao (M'99) received the Ph.D. degree from the University of Bristol, Bristol, U.K. in 1998.

From 1998 to 2000, he was a Post-Doctoral Research Fellow with the School of Electrical and Electronic Engineering, University of Birmingham, Birmingham, U.K. In May 2000, he joined the Antenna Engineering Group, Queen Mary College, University of London, London, U.K., initially as a Lecturer and currently as a Reader in antenna and electromagnetics. He coedited a book, contributed two book chapters, and authored or coauthored over 60 technical papers. His research interests are computational electromagnetics, on-body radio propagations, active integrated antennas, electromagnetic-bandgap structures, and microwave metamaterials.

Dr. Hao is a member of Institution of Electrical Engineers (IEE), U.K. He is also a member of the Technical Advisory Panel of the IEE Antennas and Propagation Professional Network and a member of the Wireless Onboard Spacecraft Working Group, European Space Research and Technology Centre (ESTEC), European Space Agency (ESA). He was a session organizer and chair for various international conferences and also a keynote speaker at ANTEM 2005, Saint-Malo, France.

Akram Alomainy (S'03) received the M.Eng. degree in communication engineering from Queen Mary College, University of London (QMUL), London, U.K., in 2003, and is currently working toward the Ph.D. degree at QMUL.

In September 2003, he commenced his research studies with the Electronic Engineering Department, QMUL. He has authored or coauthored numerous conference and journal publications. His current research interests include, small and compact antennas for WBANs, radio propagation characterization and modeling for body-centric networks, antenna interactions with human body, and computational electromagnetic and advanced antenna enhancement techniques.

Mr. Alomainy has attended a number of established international conferences.

Clive Parini (M'96) received the B.Sc. (Eng.) and Ph.D. degrees from Queen Mary College, University of London, London, U.K., in 1973 and 1976, respectively.

He then joined ERA Technology Ltd., Surrey, U.K., where he was involved with the design of microwave feeds and offset reflector antennas. In 1977, he returned to Queen Mary College, University of London, where is currently Professor of antenna engineering and heads the Communications Research Group. He has authored or coauthored over 100 papers on research topics including array mutual coupling, array beam forming, antenna metrology, microstrip antennas, application of metamaterials, millimeter-wave compact antenna test ranges, and millimeter-wave integrated antennas. He is an Honorary Editor of *Proceedings IEEE—Microwaves, Antennas, and Propagation*.

Prof. Parini is a Fellow of the Institution of Electrical Engineers (IEE), U.K. He is currently the chairman of the IEE Antennas and Propagation Professional Network Executive Team. He has been on the Organizing Committee for a number of international conferences and, in 1991, was the vice chairman and, in 2001, the chairman of the IEE International Conference on Antennas and Propagation. In January 1990, he was a corecipient of the IEE Measurements Prize for his work on near-field reflector metrology.